Anti-inflammation treatment for protection of hepatocytes and amelioration of hepatic fibrosis in rats

SHI FENG[1*], HUAN TONG[2*], JIN-HANG GAO[2], SHI-HANG TANG[2], WEN-JUAN YANG[2], GUI-MING WANG[3], HONG-YING ZHOU[3] and SHI-LEI WEN[1]

[1]Key Laboratory of Brain Science Research and Transformation in Tropical Environment of Hainan Province, Hainan Medical University, Haikou, Hainan 571199; [2]Division of Peptides Related with Human Diseases, State Key Laboratory of Biotherapy, West China Hospital, Sichuan University; [3]Department of Human Anatomy, West China School of Basic Medical Science and Forensic Medicine, Sichuan University, Chengdu, Sichuan 610041, P.R. China

Received September 18, 2020; Accepted June 11, 2021

DOI: 10.3892/etm.2021.10647

Abstract. Chronic inflammation is considered as an important pathophysiologic mechanism of hepatic cirrhosis, which induces hepatocyte injury and activates hepatic stellate cells (HSCs), thus resulting in hepatic fibrosis. Previous studies have reported that cyclooxygenase-2 (COX-2) inhibitor can effectively treat liver fibrosis, while somatostatin (SST) analogues inhibit the activation of HSCs. The present study aimed to investigate the effects of a COX-2 inhibitor, celecoxib, combined with a SST analogue, octreotide, for protection of hepatocytes and prevention of fibrosis in a rat model of hepatic fibrosis. Therefore, a hepatic fibrosis rat model was established following peritoneal injection of thioacetamide (TAA), and the rats were then treated with a combination of celecoxib and octreotide (TAA + C). Immunohistochemistry and western blotting assays were used to assess the expression levels of proteins associated with inflammation, epithelial-mesenchymal transition (EMT), proliferation, apoptosis and autophagy. H&E staining, transmission electron microscopy and scanning electron microscopy were used to evaluate the destruction of hepatocytes. Masson's Trichrome and Sirius Red were used to measure the degree of liver fibrosis. The results demonstrated that, compared with those of the control group, the degree of liver fibrosis and the expression of the intrahepatic inflammation factors were aggravated in the TAA group. Furthermore, the apoptosis rate, EMT and autophagy of hepatocytes were also increased in the TAA group. However, treatment with TAA + C restored the aforementioned increased levels compared with the TAA group. In conclusion, treatment of rats with the combination of celecoxib and octreotide could attenuate the progress of hepatic fibrosis via protection of hepatocytes by reducing apoptosis, EMT and autophagy in hepatocytes.

Correspondence to: Dr Shi-Lei Wen, Key Laboratory of Brain Science Research and Transformation in Tropical Environment of Hainan Province, Hainan Medical University, 3 Xueyuan Road, Haikou, Hainan 571199, P.R. China
E-mail: wenshl2005@126.com

Dr Hong-Ying Zhou, Department of Human Anatomy, West China School of Basic Medical Science and Forensic Medicine, Sichuan University, 17 South Renmin Road, Chengdu, Sichuan 610041, P.R. China
E-mail: eaglezhyxzy@163.com

*Contributed equally

Abbreviations: EMT, epithelial-mesenchymal transition; HSCs, hepatic stellate cells; IHC, immunohistochemistry; MT, Masson's trichrome; RT-qPCR, reverse transcription-quantitative PCR; SD, Sprague-Dawley; SST, somatostatin; TAA, thioacetamide; TEM, transmission electron microscopy; OD, optical density

Key words: hepatic fibrosis, inflammation, hepatocyte, celecoxib, octreotide

Introduction

Cirrhosis is induced by several types of chronic or repeated hepatic damages and its incidence is increasing worldwide (1). Although numerous attempts have been made to prevent and/or reverse liver fibrosis in the past decade, liver transplantation still remains the only effective therapy (2). The effect of progressive inflammation on hepatic fibrosis has been widely investigated in previous years, and this not only induces chronic hepatocyte injury, but also increases the activation and proliferation of hepatic stellate cells (HSCs) (3). HSCs can transform into myofibroblasts (MFBs) to synthesize fibers, resulting in hepatic fibrosis and even cirrhosis (4). In addition, the epithelial-mesenchymal transition (EMT) of hepatocytes can be induced by inflammation via the upregulation of growth factors, particularly TGF, thus resulting in the transformation of hepatocytes into MFBs and progression of liver fibrosis (5). Although hepatocyte EMT has been refuted by a series of lineage tracing experiments (6,7), our previous study demonstrated *in vivo* that during hepatic fibrosis the epithelial biomarkers on hepatocytes were lost and the mesenchymal biomarkers were increased (8), indicating that hepatocytes

could be an important source of fibers during hepatic fibrosis. It has also been reported that autophagy is involved in liver fibrosis and facilitates its progress (9,10). On the other hand, prostaglandins can exacerbate inflammation (11), whereas cyclooxygenase-2 (COX-2) acts as a key rate-limiting enzyme to catalyze them (12). The high expression levels of COX-2 in fibrotic livers indicated that COX-2 could be considered as a key regulator in accelerating hepatitis (12).

In the present study, thioacetamide (TAA), a classic drug against liver damage, was used to induce hepatic fibrosis in rats (13). Subsequently, rats with hepatic fibrosis were co-treated with celecoxib and octreotide to investigate their effects on hepatocyte EMT, apoptosis and autophagy. Additionally, the hepatic fibrosis process was monitored to evaluate the effects of celecoxib and octreotide on protection of hepatocytes during fibrosis. Somatostatin (SST) exerts immunomodulatory, antisecretory and antiproliferative functions via binding to SST receptors (SSTR1-5), while octreotide is an analogue of SST (14-16). The present study hypothesized that the combination of octreotide with celecoxib could be considered as an efficient approach for protection of hepatocytes and attenuation of hepatic fibrosis.

Materials and methods

Animal studies. A total of 36 male Sprague-Dawley (SD) rats (age, 12 weeks; weight, 200-230 g) were purchased from West China Medical Experimental Animal Center, Sichuan University (Chengdu, Sichuan, China). All animals were housed in a specific pathogen-free facility (temperature, 25±2˚C; humidity, 50±10%) with a 12/12-h light/dark cycle and free access to chow and water. The animal procedures were approved by the Animal Use and Care Committee of the Sichuan University (approval no. K2015004; Chengdu, Sichuan, China).

Liver fibrosis model was induced by intraperitoneal injection (i.p.) of 200 mg/kg TAA (40 mg/ml dissolved in sterile saline; Sigma-Aldrich; Merck KGaA) every 3 days for 16 weeks (17). Animals were randomized into control, TAA and TAA + celecoxib + octreotide (TAA + C) groups, with 12 animals in each group. Rats in the control group were treated with sterile saline (1 ml; i.p.) every 3 days as a vehicle control. Rats in the TAA group were treated with TAA (200 mg/kg dissolved in sterile saline; i.p.) every 3 days and sterile saline daily (1 ml/kg; s.c.; twice per day), while those in the TAA + C group were given a combination of TAA, celecoxib (gastric gavage; 20 mg/kg/day; Pfizer, Inc.) and octreotide (s.c.; 50 μg/kg/day; Novartis International AG). In the TAA + C group, celecoxib and octreotide were given to rats together with TAA synchronously from the beginning of the experiment. During the modeling, one rat died in each of the TAA and TAA + C groups, while no death was observed in the control group. All animals were sacrificed by cardiac exsanguination under general anesthesia with sodium pentobarbital (30 mg/kg; i.p.).

Morphology detection of liver tissues. The gross morphology of the liver was examined to evaluate hepatic fibrosis. Liver tissues were fixed in 4% neutral buffered paraformaldehyde for 48 h at 4˚C. Tissues were dehydrated using an ascending alcohol series at 70, 80, 90, 95 and 100%. Degreasing was carried out using xylene for 45 min at room temperature. Subsequently, samples were infiltrated in paraffin for 30 min at 65˚C three times. Finally, tissues were embedded in paraffin wax and sectioned into 4-μm thick sections.

Following dewaxing and rehydration with xylene, and rehydration with a descending alcohol series, liver slides were stained with hematoxylin for 5 min at room temperature. Slides were subsequently washed with acid alcohol (1% hydrochloric acid:70% alcohol) for 15 sec at room temperature and immerged in ammonia solution for 10 sec at room temperature. Slides were stained with 1% eosin for 2 min at room temperature. The slides were subsequently dehydrated using an ascending alcohol series at 90, 95 and 100% for 2 min at room temperature at each stage, followed by incubation in xylene twice for 3 min each. Sections were sealed using synthetic resin and observed using a light microscope (Eclipse Ti2-A; Nikon Corporation).

To evaluate hepatic nodules and fibrotic septa, sections were stained with Masson's Trichrome and Sirius Red. For Masson's Trichrome, following deparaffinization and hydration in water, slides were subsequently treated with Trichrome Stain kit (cat. no. ab150686; Abcam) Briefly, slides were incubated in Bouin's Fluid for 60 min at 60˚C followed by a 10-min cooling period. Slides were washed in water until sections were completely clear, and slides were stained with working Weigert's Iron Hematoxylin for 5 min, followed by washing in water for 2 min. Biebrich Scarlet and Acid Fuchsin solution was added to slides for 15 min, followed by washing in water. Slides were differentiated in Phosphomolybdic and Phosphotungstic Acid solution for 15 min. Applied Aniline Blue solution was added to slides for 10 min followed by washing in distilled water. 1% Applied Acetic Acid solution was added to slides for 3-5 min, followed by dehydration in an ascending alcohol series. Slides were incubated in xylene and sealed in synthetic resin. Subsequently, five images per section were randomly captured using a light microscope (Eclipse Ti2-A; Nikon Corporation; magnification, x100) from each liver tissue. The area of fibers was evaluated using Image-Pro Plus 6.0 software (CAD/CAM Services, Inc.) and fibrosis was assessed using the Ishak scoring system (scores, 0-6; higher score denotes more severe fibrosis) (18). The standards of Ishak's Score were as follows: 0, no fibrosis; 1, fibrous expansion of some portal areas, with or without short fibrous septa; 2, fibrous expansion of most portal areas, with or without short fibrous septa; 3, fibrous expansion of most portal areas with occasional portal to portal bridging; 4, fibrous expansion of portal areas with marked portal to portal bridging as well as portal to central bridging; 5, marked bridging with occasional nodules; 6, cirrhosis, probable or definite.

Sirius Red staining was applied to verify the results of the Masson's Trichrome staining. Following deparaffinization and hydration in water, slides were subsequently treated as follows: Stained in 0.1% Sirius red and saturated picric acid for 10 min at room temperature, followed by washing in water. Slides were dehydrated using an ascending alcohol series, incubated in Xylene and sealed in synthetic resin. Finally, images of sections were randomly captured using a light microscope as previously described.

For electron microscopy detection, animals were transcardially perfused with 0.01 M PBS (pH 7.4), anesthetized with sodium pentobarbital at 30 mg/kg i.p., and transcardially perfused with 2% paraformaldehyde and 2.5% glutaraldehyde mixed solution. The next steps differed between distinct types of electron microscopy. Therefore, for scanning electron microscopy (SEM), liver tissues were immediately frozen with liquid nitrogen for 20 min at -196˚C, smashed into pieces and fixed in 2.5% glutaraldehyde overnight at 4˚C. After dehydration using an ascending alcohol series and sputter coating using gold, the surface ultrastructure of liver tissues was observed under a SEM system (JSM-7500F; JEOL Ltd.). For transmission electron microscopy (TEM), liver tissues were cut into cubes of ~1 mm^3 and fixed with 2.5% glutaraldehyde at 4˚C overnight, and fixed again in 1% phosphate-buffered osmium tetroxide (0.1 M; pH 7.2) for 1 h at room temperature. Sections were dehydrated in a graded alcohol solution, and embedded with Epon 812 resin overnight at 35˚C, 12 h at 45˚C and 24 h at 60˚C, in sequence. Tissues were cut into 70-nm sections followed by staining with uranyl acetate for 10 min at room temperature and lead citrate for 5 min at room temperature. Sections were observed using a TEM system (H-600IV; Hitachi, Ltd.) and images were obtained using Gatan Microscopy Suite 64-bit 3.2 (Gatan, Inc.).

Reverse transcription-quantitative PCR (RT-qPCR). Total RNA was extracted from hepatic tissues using TRIzol® reagent (Invitrogen; Thermo Fisher Scientific, Inc.) according to the manufacturer's instructions. The purity and concentration of RNA was measured using the OD at 260 nm and the 260/280 nm ratio was calculated. RNA with a 260/280 ratio between 1.8-2.0 was used for subsequent experiments. cDNA was synthesized using a cDNA Reverse Transcription kit (Fermentas; Thermo Fisher Scientific, Inc.) under the following conditions: 42˚C for 60 min, 70˚C for 5 min and 4˚C for 30 min. Subsequently, qPCR was performed using a SYBR® Green qPCR supermix (Bio-Rad Laboratories, Inc.) on a CFX96 qPCR system (Bio-Rad Laboratories, Inc.). The following thermocycling conditions were used: Initial denaturation at 95˚C for 3 min; followed by 40 cycles of denaturation at 95˚C for 30 sec, and annealing at 60˚C for 30 sec. The primer sequences used are listed in Table SI. The relative mRNA expression levels of the target genes were calculated using the $2^{-\Delta\Delta Cq}$ method (19) and normalized to that of GAPDH.

Immunohistochemistry (IHC) assessment. After deparaffinization and rehydration of liver slides, antigen retrieval was performed using citrate buffer solution (0.01 M; pH 6.0) in an electric oven ~95˚C for 15 min. After rinsing with PBS, the slides were incubated in 3% H_2O_2 for 10 min at room temperature. The slides were subsequently blocked with 5% goat serum (cat. no. ZLI-9021; OriGene Technologies, Inc.) for 15 min at 37˚C. Following incubation with the primary antibody overnight at 4˚C, a Secondary Antibody kit was applied according to the manufacturer's instructions (cat. nos. SP-9001; SP-9002; PV-9003; all purchased from ZSGB-BIO, Co., Ltd.) Sections were incubated with biotin-conjugated secondary antibody for 30 min at 37˚C followed by incubation with HRP-conjugated avidin for 30 min at 37˚C. IHC reactions were developed using DAB Horseradish Peroxidase Color Development kit (cat. no. ZLI-9018; ZSGB-BIO, Co., Ltd.), and nuclei were counterstained with hematoxylin for 3 min at room temperature. The slides were dehydrated using an ascending alcohol series at 90, 95 and 100% for 2 min at each stage, followed by incubation in xylene twice for 3 min each. Finally, tissue sections were sealed with neutral resins. The images of the sections were captured using a light microscope as previously described.

The primary antibodies used for IHC analysis were listed in Table SII. The cell number of positive PCNA was counted in five randomly captured images per slide (magnification, x400), while the optical density (OD) of SST and cleaved caspase-3 was measured using the Image-Pro Plus v 6.0 analysis software (Media Cybernetics, Inc.). The relative OD value of the control group was considered to be 1, and the relative OD values of the other two groups were obtained based on the ratios of the original OD values of the other two groups to that of the control group, separately.

Western blot analysis. Liver tissues were homogenized in liquid nitrogen, and whole proteins were extracted using ice-cold RIPA buffer (Beyotime Institute of Biotechnology). Protein concentrations were quantified using a BCA assay (cat. no. PA115-01; Tiangen Biotech Co, Ltd.). Protein samples were added to 5X loading buffer, heated in boiling water for 5 min, and then equal amounts of proteins (30 μg) from each sample were resolved by 12 or 15% SDS-PAGE, and transferred to PVDF membranes (MilliporeSigma). Membranes were blocked with 5% non-fat powdered milk in TBS (20 mM Tris-HCl pH 7.5, 150 mM NaCl) with 0.1% Tween-20 for 1 h at room temperature. The membranes were subsequently incubated with primary antibodies at 4˚C overnight followed by secondary antibody incubation for 1 h at 37˚C. The targeting proteins were detected by chemiluminescence using an ECL kit (Beyotime Institute of Biotechnology). Protein expression levels were normalized to GAPDH and analyzed using Quantity_One_v462_PC (Bio-Rad Laboratories, Inc.). The antibodies used for western blot analysis were listed in Table SII.

ELISA for serum prostaglandin E2 (PGE2). Blood was collected from the right femoral artery of rats and centrifuged at 1,000 x g for 10 min at room temperature to obtain blood serum. The concentration of serum PGE2 was quantified using an ELISA Kit for PGE2 (cat. no. CEA538Ge; Wuhan USCN Business Co., Ltd.) according to the manufacturer's instructions. Plates were read using a Thermo microplate reader (Thermo Fisher Scientific, Inc.) at a wavelength of 450 nm.

TUNEL assay. TUNEL staining was applied using 4-μm thick paraffin sections of liver tissues, obtained as previously described. This test was performed using an *In Situ* Cell Death Detection kit (cat. no. 11684817910; Roche Diagnostics GmbH) according to the manufacturer's instructions. Following deparaffinization and rehydration, the sections incubated in permeabilization solution containing 0.1% Triton X-100 and 0.1% sodium citrate for 20 min at room temperature, followed by washing with PBS. Sections were incubated with 3% hydrogen peroxide in PBS for 5 min to inhibit endogenous peroxidase activity and rinsed with PBS. Sections were subsequently

incubated with a TUNEL reaction mixture for 1 h at 37˚C, rinsed with PBS, and incubated with converter-POD for 30 min at 37˚C. Sections were washed with PBS and stained with DAB (cat. no. ZLI-9018; Origene Technologies, Inc.) and rinsed with PBS. Nuclei were stained with hematoxylin staining solution for 5 min at room temperature, dehydrated using an ascending alcohol series and incubated with xylene. Finally, tissue sections were sealed with neutral resins. The sections were observed using a light microscope and the TUNEL-positive cells were counted using Image-Pro Plus v 6.0 analysis software, as previously described.

Statistical analysis. All data were presented as the mean ± standard deviation. The results were analyzed using SPSS 19.0 software (IBM Corp.), and one-way ANOVA was applied to compare differences among multiple groups followed by Tukey's post hoc test. $P<0.05$ was considered to indicate a statistically significant difference.

Results

Celecoxib and octreotide mitigate hepatic inflammation. Compared with those in the control group, the protein expression levels of COX-2, IL-6 and TNF-α were increased in the TAA group (Fig. 1E). However, intrahepatic inflammation was attenuated in the TAA + C group compared with the TAA group, as demonstrated by the downregulation of COX-2, IL-6 and TNF-α. In addition, the OD value of SST in liver tissues and the serum levels of PGE2 in the TAA + C group were notably decreased compared with those in the TAA group (Fig. 1C and D). Moreover, the mRNA expression level of COX-2 was decreased in the TAA + C group compared with the TAA group, but this result was not significant.

Celecoxib and octreotide protect the morphology of hepatocytes. Cytoplasmic vacuolization and nucleus pyknosis in hepatocytes, irregular arranged hepatic cords and collapsed hepatic sinusoids were observed in the TAA group. However, these changes were not apparent in the TAA + C group (Fig. 2A).

TEM images further revealed numerous irregular, even lysed, mitochondria, as well as an increased number of vesicles in the TAA group. However, in the TAA + C group, restoration of the aforementioned findings was observed, although partially broken and incomplete mitochondria could still be found (Fig. 2B). Additionally, observation by SEM revealed that microvilli in the TAA + C group were similar to those in the control group. However, microvilli in the TAA group were shorter, thinner and sparser, suggesting more severe hepatocyte damage.

Co-treatment with celecoxib and octreotide attenuates hepatocyte EMT. The expression levels of EMT-related markers, including the TGF-β1/Smad signaling pathway factors, TGF-β1, phosphorylated (p)-Smad2, Smad2, 3, 4, and 7, Snail1, E-cadherin and N-cadherin, were determined in liver tissues by RT-qPCR, IHC and western blot analysis (Fig. 3). The mRNA expression levels of Smad3, Smad4 and Smad7 were not significantly different among the three groups ($P>0.05$; Fig. 3B). Compared with those in the control group, the mRNA levels of the pro-EMT markers, TGF-β1, Smad2 and Snail1, were notably increased in the TAA group, and the mRNA level of E-cadherin was significantly decreased in the TAA group (Fig. 3B). Furthermore, the levels of TGF-β1, Smad2 and Snail1 were markedly reduced in the TAA + C group compared with the TAA group. Finally, E-cadherin was upregulated in the TAA + C group compared with the TAA group.

The western blot analyses results revealed that the levels of the pro-EMT markers, including TGF-β1, the ratio of p-Smad2 to/Smad2, Snail1 and N-cadherin in hepatocytes of the TAA group were markedly higher compared with those in the control group (Fig. 3C). Similar results were revealed by IHC (Fig. 3A). On the contrary, the expression levels of the epithelial marker E-cadherin in the TAA group were decreased compared with those in the control group ($P<0.01$). Compared with the TAA group, TGF-β1, the ratio of p-Smad2/Smad2, Snail1 and N-cadherin were markedly downregulated and E-cadherin was notably upregulated in the TAA + C group ($P<0.05$ or $P<0.01$).

Celecoxib and octreotide have no effect on hepatocyte proliferation. The protein expression of proliferating cell nuclear antigen (PCNA) was evaluated by IHC staining by measuring the PCNA-positive cell number. Hepatocytes were identified basing on their morphology and the PCNA-positive hepatocytes were counted (Fig. 4A and B). There were no significant difference in the total number of PCNA-positive hepatocytes among the control, TAA and TAA + C groups.

Celecoxib and octreotide affect hepatocyte apoptosis. The mRNA expression levels of the apoptosis-related factors, bax, caspase-3 and bcl-2 were measured by RT-qPCR to evaluate the intrahepatic apoptosis status (Fig. 4D). Among all experimental groups, no significant differences were observed in the mRNA expression levels of bax and bcl-2. However, the mRNA expression levels of caspase-3 in the control group were significantly decreased compared with those in the other two groups. The highest levels of caspase-3 were observed in TAA group, which were also significantly higher compared with those in the TAA + C group. To confirm the aforementioned findings, the protein expression level of cleaved caspase-3 was evaluated via IHC on slides. The results were consistent with those observed in the RT-qPCR analysis (Fig. 4C and E).

The TUNEL staining results demonstrated that the number of TUNEL-positive hepatocytes was statistically higher in the TAA group compared with the control group (33.71±6.74 vs. 22.69±4,55; Fig. 4C and F). In addition, the number of TUNEL-positive cells was reduced in the TAA + C group (27.23±7.45) compared with the TAA group (33.71±6.74); however, the difference was not statistically significant.

Co-treatment with celecoxib and octreotide slightly attenuates hepatocyte autophagy. To investigate the effect of the combined treatment with celecoxib and octreotide on inhibiting hepatocyte autophagy, the expression levels of the autophagy-related markers beclin-1, P62, LC3A and LC3B were assessed by IHC and western blot analysis (Fig. 5). The IHC assay results demonstrated that positive signal was mainly observed in hepatocytes, while the mesenchyme was almost

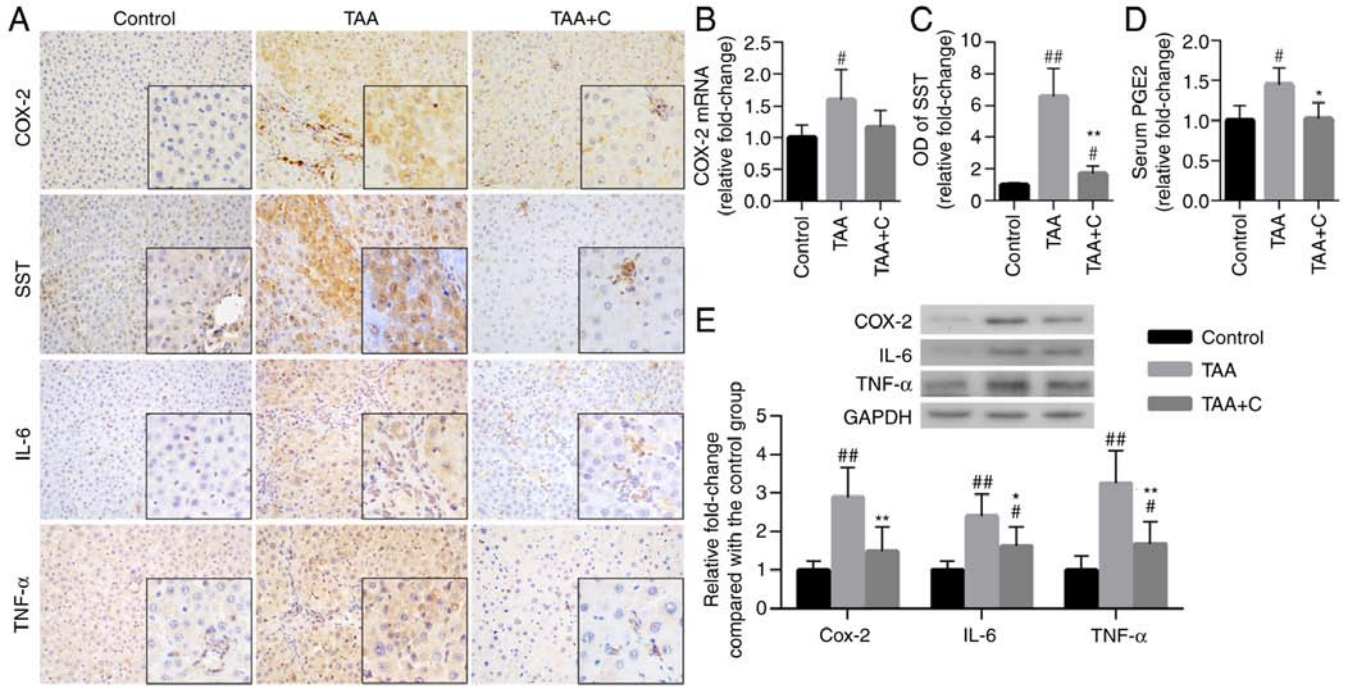

Figure 1. Treatment with celecoxib and octreotide attenuates hepatic inflammation. (A) Immunohistochemical staining of COX-2, SST, IL-6 and TNF-α in liver sections (magnification, x400; insert, x1,000). (B) COX-2 mRNA expression was measured in hepatic tissues by reverse transcription-quantitative PCR (n=11/group). (C) OD values of SST (n=6). (D) Serum secretion levels of PGE2 were detected by ELISA (n=11). (E) Relative protein expression levels of COX-2, IL-6 and TNF-α were determined in liver tissues by western blot analysis (n=6). $^{\#}$P<0.05 and $^{\#\#}$P<0.01 vs. control group; *P<0.05 and **P<0.01 vs. TAA group. COX-2, cyclooxygenase-2; OD, optical density; PGE2, prostaglandin E2; SST, somatostatin; TAA, thioacetamide.

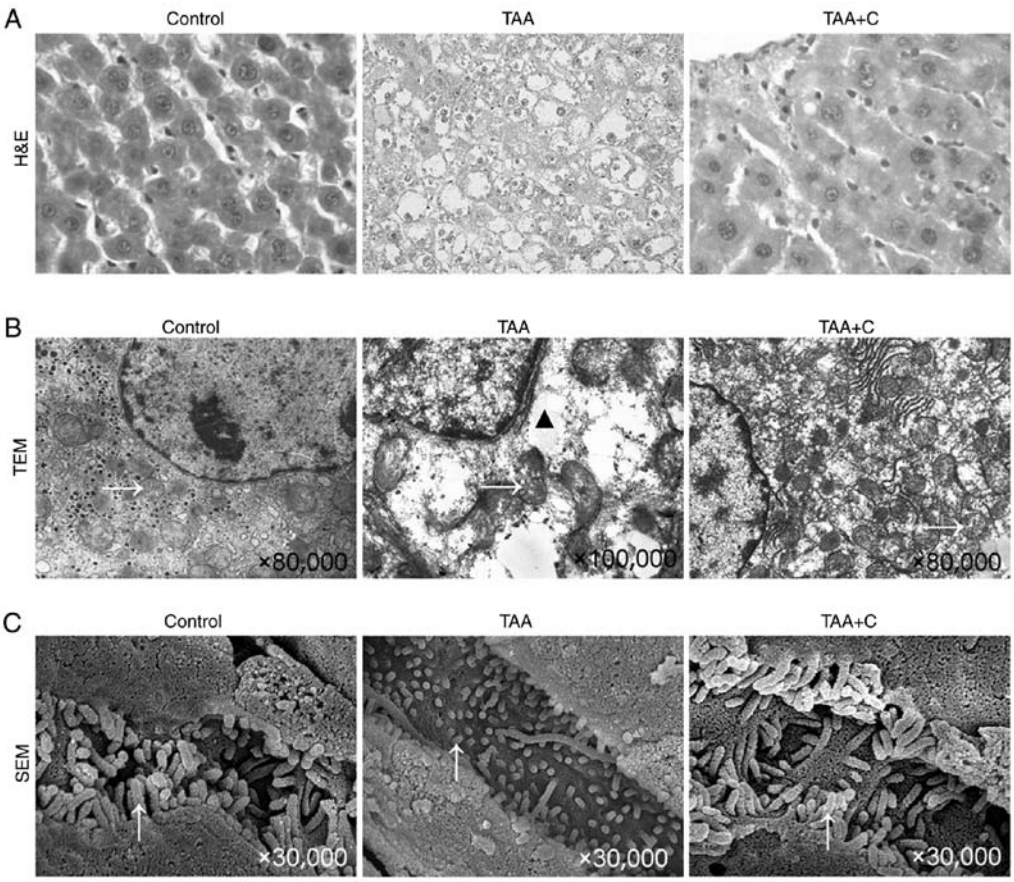

Figure 2. Treatment with celecoxib and octreotide protects the morphology and microstructure of hepatocytes. (A) Liver tissue sections stained with H&E (magnification, x1,000). (B) Microstructure of hepatocytes observed by TEM. (C) Microvilli of hepatocytes were observed by SEM. Arrow pointing up, microvilli of hepatocytes; triangle, vesicles; arrow pointing right, mitochondrion. TEM, transmission electron microscopy; SEM, scanning electron microscopy; TAA, thioacetamide.

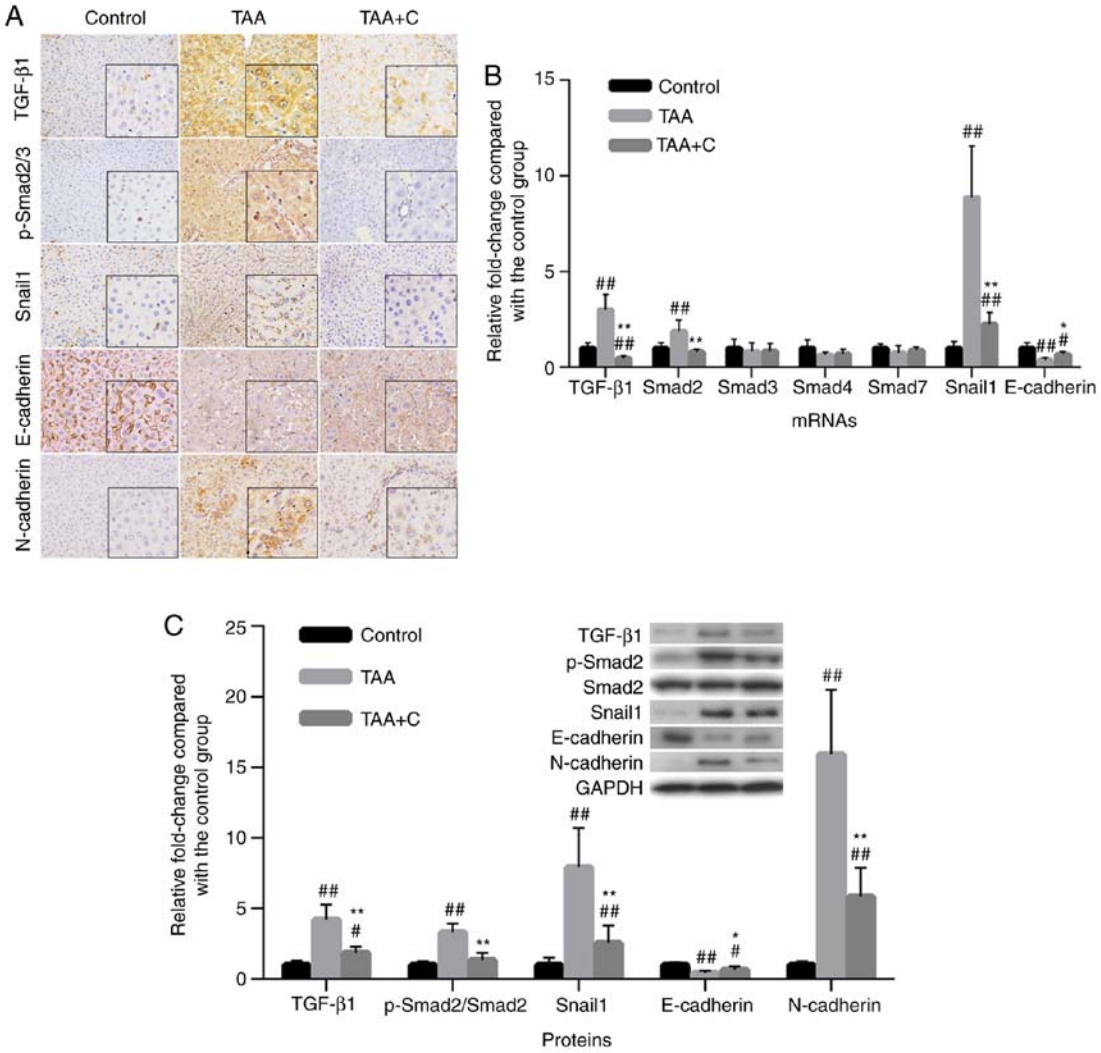

Figure 3. Treatment with celecoxib and octreotide attenuates epithelial-mesenchymal transition. (A) Immunohistochemical staining of TGF-β1, p-Smad2/3, Snail1, E-cadherin and N-cadherin in liver sections (magnification, x400; insert, x1,000). (B) Relative TGF-β1, Smad2, Smad3, Smad4, Smad7, Snail1 and E-cadherin mRNA expression was quantified by reverse transcription-quantitative PCR (n=11). (C) Relative protein expression levels of TGF-β1, Snail1, E-cadherin and N-cadherin, and the ratio of p-Smad2/Smad2 in liver tissues were determined by western blot analysis (n=6). $^{\#}$P<0.05 and $^{\#\#}$P<0.01 vs. control group; *P<0.05 and **P<0.01 vs. TAA group. p-Smad2, phosphorylated Smad2; TAA, thioacetamide.

negative. All factors tested were upregulated in the TAA and TAA + C groups compared with the control group (Fig. 5A). Furthermore, compared with the control group, the western blotting results demonstrated that beclin-1, P62 and LC3B were notably upregulated in the TAA group, P62 and LC3B were notably upregulated in the TAA + C group, while the TAA group exhibited increased expression levels compared with the TAA + C group. However, a statistically significant difference between these groups was only observed for LC3B expression (Fig. 5B).

Celecoxib and octreotide attenuate liver fibrosis. Based on the gross features of liver and histological staining, the TAA group exerted the typical morphological characteristics of fibrosis, with large nodules on the surface and complete interlobular fibrotic septa (Fig. 6). In the TAA + C group, the size of nodules on the surface was much smaller and the interlobular fibrotic septa were incomplete (Fig. 6A and B). The statistical analysis revealed that the fibrotic area and the Ishak's score in the TAA and TAA + C groups were significantly higher compared with those in the control group (P<0.01), and those in the TAA group were markedly higher than those in the TAA + C group (P<0.05 or P<0.01; Fig. 6C and D).

Discussion

In the present study, a hepatic fibrosis rat model induced by TAA was established to investigate the effects of celecoxib and octreotide on hepatic cells and liver fibrogenesis. Co-treatment with these two drugs exhibited marked anti-inflammatory effects, thereby strongly attenuating intrahepatic inflammation. Furthermore, the drugs alleviated the pathological injury and apoptosis of hepatocytes, and inhibited EMT and hepatocyte autophagy, thus resulting in the inhibition of hepatic fibrosis.

It is widely accepted that persistent inflammation serves an important role in triggering liver fibrosis (20). In addition, the eruption of chronic inflammation always induces liver fibrosis (1). Therefore, anti-inflammatory reactions are considered as an efficient approach for inhibiting fibrogenesis (21). Our previous study demonstrated that celecoxib could improve the integrity

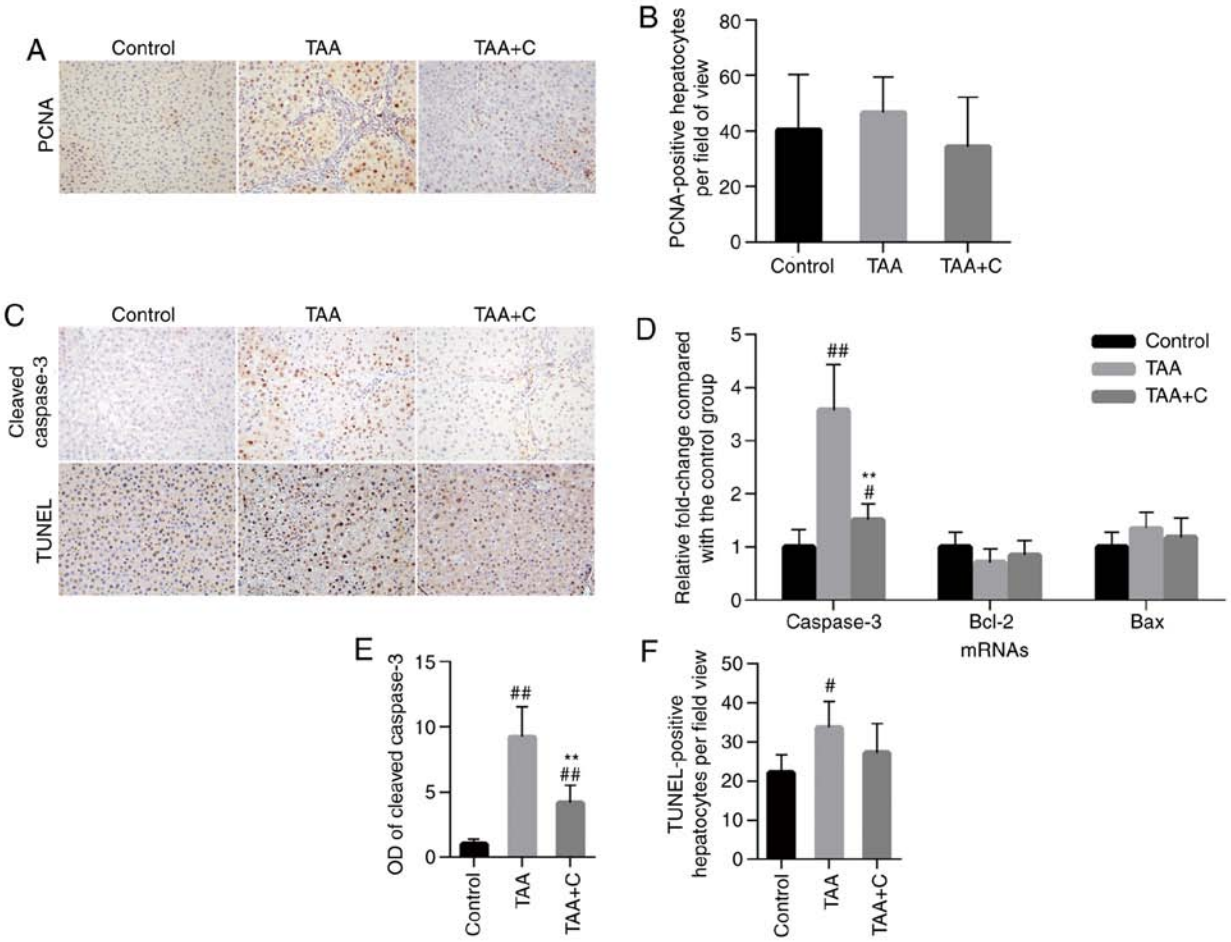

Figure 4. Effects of celecoxib and octreotide on intrahepatic cell proliferation and apoptosis. (A) Immunohistochemical staining of PCNA in liver sections (magnification, x400). (B) Number of PCNA-positive hepatocytes (n=11). (C) Immunohistochemical staining for cleaved caspase-3 and TUNEL staining. (D) Relative caspase-3, bax and bcl-2 mRNA expression levels were measured by reverse transcription-quantitative PCR (n=11). (E) OD values of cleaved caspase-3 (n=6). (F) Number of TUNEL-positive hepatocytes (n=6). $^{\#}$P<0.05 and $^{\#\#}$P<0.01 vs. control group; **P<0.01 vs. TAA group. OD, optical density; PCNA, proliferating cell nuclear antigen; TAA, thioacetamide.

of the intestinal epithelial barrier, block the inflammatory transport from the gut into the liver, and ameliorate the progress of hepatic fibrosis (22). However, other studies reported different results regarding the treatment of liver fibrosis with celecoxib or SST analogues (23-26). A number of studies failed to alleviate hepatic fibrosis induced by CCl_4 (25,26); however, these findings could be due to treatment with extremely high doses of hepatoxin drugs, which could mediate more severe damages, and low doses of celecoxib, which could be insufficient to inhibit the excessive inflammatory responses in the liver (25,26). In addition, both celecoxib and SST analogues failed to treat liver fibrosis induced by bile duct ligation (23,24). In the present study, liver fibrosis in rats was slowly induced, and the doses of celecoxib and octreotide were sufficient to attenuate the expression of inflammatory factors, such as IL-6 and TNF-α, thus providing strong anti-inflammatory and anti-fibrosis effects.

Several studies have reported that EMT usually occurs in the liver during liver fibrosis (27,28). In the inflammatory microenvironment, the TGF-β1/Smads signaling pathway is upregulated and activated, and is generally considered as one of the crucial regulators of EMT (29). The Snail1 transcriptional factor serves a key role in the control of EMT and fibroblast activation (30). In the present study, along with the upregulation of the expression levels of TGF-β1 and p-Smad2, the pro-EMT TGF-β1/Smads signaling pathway was activated in the TAA group compared with the control group. Snail1 was also markedly upregulated in the TAA group compared with the control group. Therefore, the changes in the expression levels of EMT-related biomarkers, such as the highly expressed Snail1 and N-cadherin, and the markedly downregulated E-cadherin, also supported the occurrence of hepatocyte EMT in fibrotic liver. However, studies based on genetic labeling techniques could not identify any MFBs originating from either hepatocytes or cholangiocytes (7,31). Apart from the shortcomings of the genetic labeling technique itself, it should be considered almost certain that even if hepatocytes could not be completely transformed to MFBs, they could at least lose the epithelial cell-related biomarkers and express those associated with mesenchymal cells, thus contributing to hepatic fibrosis (32). In the present study, the combination of celecoxib and octreotide reduced the activation of the TGF-β1/Smads signaling pathway, downregulated the expression levels of Snail1, and effectively alleviated hepatocyte EMT.

During the development of liver fibrosis, chronic parenchymal damages, especially hepatocyte injury, are

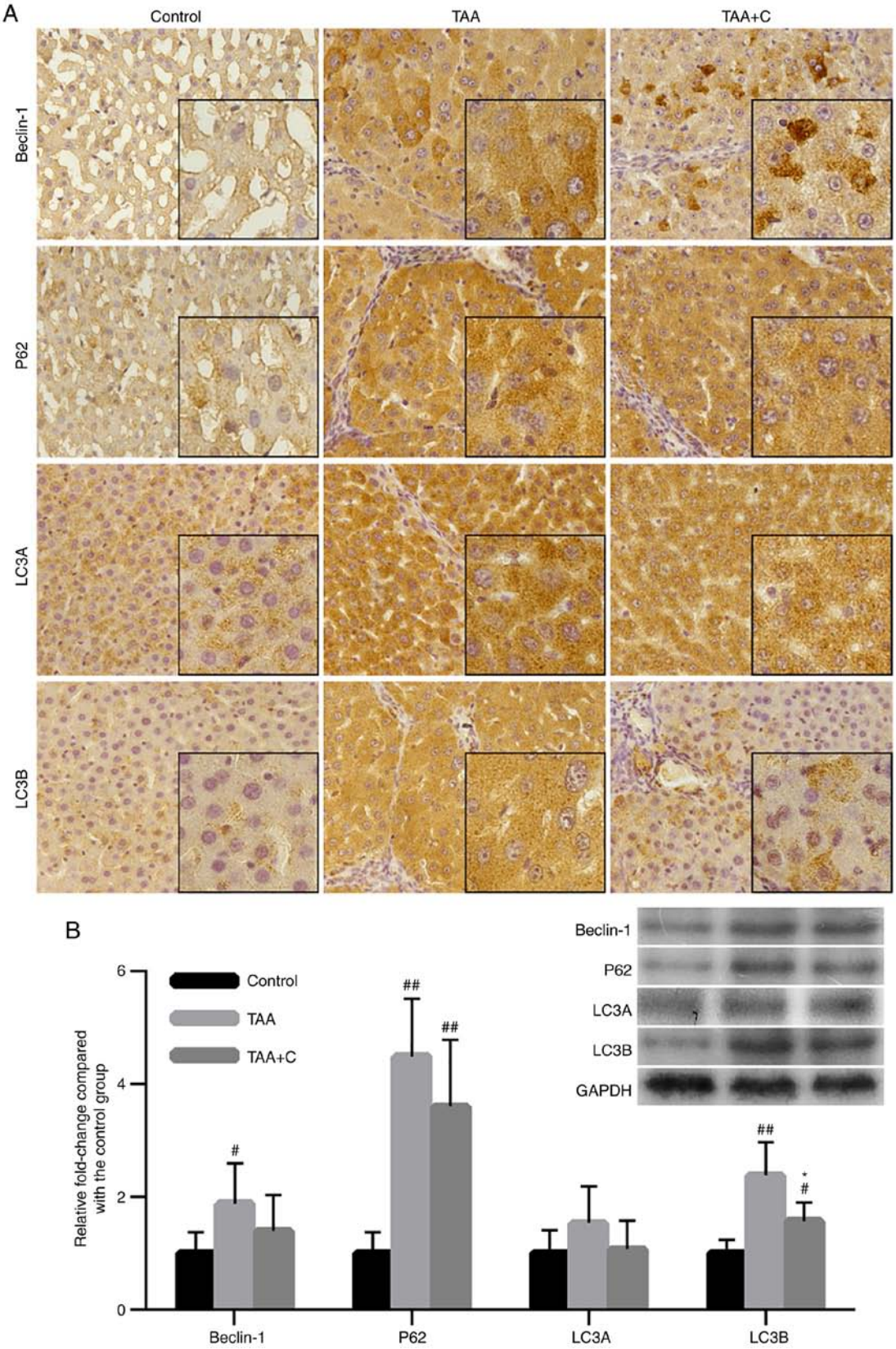

Figure 5. Treatment with celecoxib and octreotide attenuates autophagy. (A) Immunohistochemical staining of Beclin-1, P62, LC3A and LC3B in liver sections (magnification, x400; insert, x1,000). (B) Relative beclin-1, P62, LC3A and LC3B protein expression levels in liver tissues were determined by western blot analysis (n=6). $^{\#}$P<0.05, $^{\#\#}$P<0.01 vs. control group; *P<0.05 vs. TAA group. TAA, thioacetamide.

one of the main features of fibrosis (1). On the contrary, alleviating hepatocyte injury can attenuate the progression of liver fibrosis (33). According to the histopathological results, the shape, mitochondria and microvilli on the surface of hepatocytes were well protected following co-treatment with celecoxib and octreotide, indicating that the combination

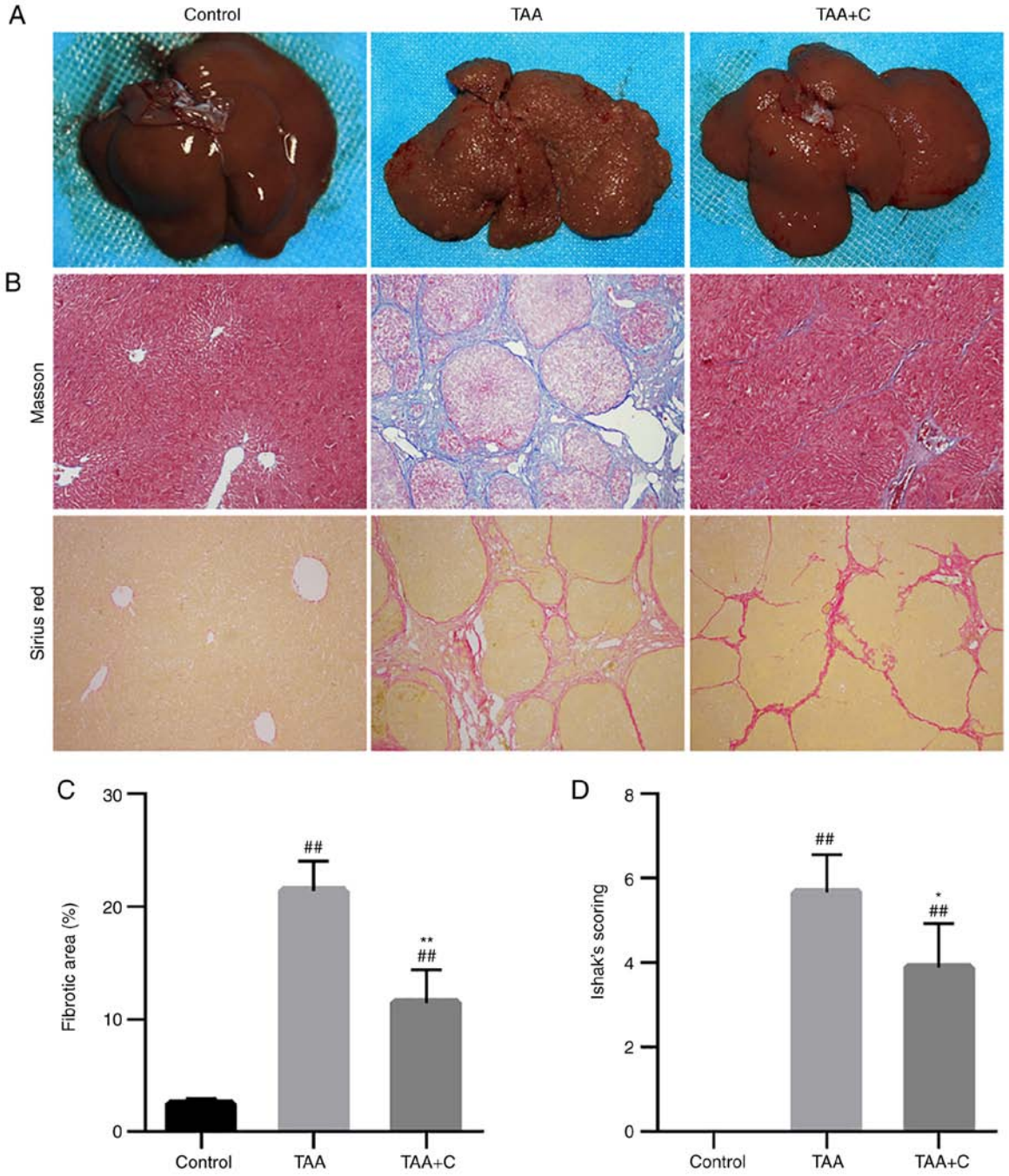

Figure 6. Treatment with celecoxib and octreotide attenuates liver fibrosis. (A) Gross views of livers. (B) MT and Sirius Red staining of liver sections (magnification, x100). (C) Fibrotic areas based on MT staining. (D) Ishak scoring system based on Sirius Red and MT staining (n=11). $^{\#\#}$P<0.01 vs. control group; *P<0.05 and **P<0.01 vs. TAA group. MT, Masson's Trichrome; TAA, thioacetamide.

of these drugs could attenuate hepatocyte injury, thus maintaining hepatocyte function and attenuating the progress of liver fibrosis.

Chronic inflammation in the liver may cause hepatocyte death, leading to the release of apoptotic bodies and other cellular debris, which are phagocytosed by HSCs, thus resulting in their activation, proliferation, differentiation and matrix deposition (34). Furthermore, high levels of TGF-β1 promote hepatocyte cell death, which contributes to liver fibrosis and later cirrhosis (35). An *in vitro* study has demonstrated that an SST analogue, sorafenib, could reduce apoptosis of murine hepatocytes (36). In the present study, the combined treatment with celecoxib and octreotide protected hepatocytes from apoptosis. This finding could be associated with the inhibition of inflammation and the TGF-β1 signaling pathway.

Autophagy is a highly conserved eukaryotic cellular self-eating catabolic pathway, which finally leads to the formation of lysosomes (37). Autophagy contributes to liver homeostasis through its role in energy balance and in the quality control of the cytoplasm, by removing misfolded proteins, damaged organelles and lipid droplets (38). The deregulation of autophagy has been associated with several liver diseases and its regulation has been recognized as a potential novel treatment strategy (39). However, the results

of studies investigating the effects of autophagy on liver fibrosis or cirrhosis are contradictory (40-44). A number of studies have suggested that autophagy prevents the development of liver fibrosis (41,44). On the other hand, other studies have demonstrated that autophagy promotes the progression of hepatic fibrosis (42,43). The aforementioned studies suggested that autophagy could regulate multiple biological processes that affect the onset hepatic fibrosis. In the present study, the expression levels of autophagy-related markers beclin-1, P62 and LC3A/B were increased in hepatocytes in the TAA group. Among these factors, LC3B is considered to be the most typical indicator for the evaluation of cellular autophagy (45). The results of the present study demonstrated that the expression levels of LC3B in the TAA + C group were notably decreased compared those in the TAA group, indicating that the level of autophagy in the TAA + C group was also lower than that in the TAA group. The present study hypothesized that co-treatment with celecoxib and octreotide could prevent intrahepatic inflammation-mediated damage to hepatocytes.

At present, etiological and symptomatic therapy are the main treatment approaches for liver cirrhosis in clinical settings (46). For example, antiviral therapy is used to treat hepatitis virus-related cirrhosis, endoscopic variceal ligation is used for treating gastrointestinal bleeding, while transjugular intrahepatic portosystemic stent-shunt is applied for treating refractory ascites and portal hypertension (47). However, the treatment for protection of hepatocytes remains under investigation. In conclusion, the present study demonstrated that inhibition of intrahepatic inflammation by co-treatment with celecoxib and octreotide could alleviate TAA-induced hepatic fibrosis in rats by protecting hepatocytes. Several mechanisms could be involved in this process, such as attenuation of pathological injury, and inhibition of hepatocyte apoptosis, EMT and autophagy. Therefore, the combined treatment with celecoxib and octreotide could reduce the progression of hepatic fibrosis and may be considered as a potential therapy approach.

Acknowledgements

Not applicable.

Funding

The present study was supported by the National Natural Science Foundation of China (grant no. 81500468) and Open Subject of Provincial Key Laboratory of Preclinical Medicine in 2020 (grant no. JCKF2020005).

Availability of data and materials

The datasets used and/or analyzed during the current study are available from the corresponding author on reasonable request.

Authors' contributions

SLW and HYZ conceived and designed the present study. SF and HT performed the experiments. JHG and GMW analyzed the data. SHT and WJY contributed to interpretation of data. SF wrote the manuscript and SLW edited the paper. SLW and HYZ confirm the authenticity of all the raw data. All authors read and approved the final manuscript.

Ethics approval and consent to participate

The experiments were approved by the Animal Use and Care Committee of Sichuan University (approval no. K2015004; Chengdu, China).

Patient consent for publication

Not applicable.

Competing interests

The authors declare that they have no competing interest.

References

1. Parola M and Pinzani M: Liver fibrosis: Pathophysiology, pathogenetic targets and clinical issues. Mol Aspects Med 65: 37-55, 2019.
2. Bodzin AS and Baker TB: Liver transplantation today: Where we are now and where we are going. Liver Transpl 24: 1470-1475, 2018.
3. Shu Y, Liu X, Huang H, Wen Q and Shu J: Research progress of natural compounds in anti-liver fibrosis by affecting autophagy of hepatic stellate cells. Mol Biol Rep 48: 1915-1924, 2021.
4. Campana L and Iredale JP: Regression of liver fibrosis. Semin Liver Dis 37: 1-10, 2017.
5. Yu K, Li Q, Shi G and Li N: Involvement of epithelial-mesenchymal transition in liver fibrosis. Saudi J Gastroenterol 24: 5-11, 2018.
6. Xie G and Diehl AM: Evidence for and against epithelial-to-mesenchymal transition in the liver. Am J Physiol Gastrointest Liver Physiol 305: G881-G890, 2013.
7. Taura K, Miura K, Iwaisako K, Osterreicher CH, Kodama Y, Penz-Osterreicher M and Brenner DA: Hepatocytes do not undergo epithelial-mesenchymal transition in liver fibrosis in mice. Hepatology 51: 1027-1036, 2010.
8. Wen SL, Gao JH, Yang WJ, Lu YY, Tong H, Huang ZY, Liu ZX and Tang CW: Celecoxib attenuates hepatic cirrhosis through inhibition of epithelial-to-mesenchymal transition of hepatocytes. J Gastroenterol Hepatol 29: 1932-1942, 2014.
9. Mallat A, Lodder J, Teixeira-Clerc F, Moreau R, Codogno P and Lotersztajn S: Autophagy: A multifaceted partner in liver fibrosis. Biomed Res Int 2014: 869390, 2014.
10. Lee YA, Wallace MC and Friedman SL: Pathobiology of liver fibrosis: A translational success story. Gut 64: 830-841, 2015.
11. Rouzer CA and Marnett LJ: Cyclooxygenases: Structural and functional insights. J Lipid Res 50 (Suppl): S29-S34, 2009.
12. Holt AP and Adams DH: Complex roles of cyclo-oxygenase 2 in hepatitis. Gut 56: 903-904, 2007.
13. Gissen P and Arias IM: Structural and functional hepatocyte polarity and liver disease. J Hepatol 63: 1023-1037, 2015.
14. Tulipano G and Schulz S: Novel insights in somatostatin receptor physiology. Eur J Endocrinol 156: S3-S11, 2007.
15. Barnett P: Somatostatin and somatostatin receptor physiology. Endocrine 20: 255-264, 2003.
16. Sun L and Coy DH: Somatostatin and its Analogs. Curr Drug Targets 17: 529-537, 2016.
17. Li X, Benjamin IS and Alexander B: Reproducible production of thioacetamide-induced macronodular cirrhosis in the rat with no mortality. J Hepatol 36: 488-493, 2002.
18. Ishak K, Baptista A, Bianchi L, Callea F, De Groote J, Gudat F, Denk H, Desmet V, Korb G, MacSween RN, *et al*: Histological grading and staging of chronic hepatitis. J Hepatol 22: 696-699, 1995.
19. Hellemans J, Mortier G, De Paepe A, Speleman F and Vandesompele J: qBase relative quantification framework and software for management and automated analysis of real-time quantitative PCR data. Genome Biol 8: R19, 2007.

20. Kartasheva-Ebertz DM, Pol S and Lagaye S: Retinoic acid: A new old friend of IL-17A in the immune pathogeny of liver fibrosis. Front Immunol 12: 691073, 2021.
21. Alegre F, Pelegrin P and Feldstein AE: Inflammasomes in liver fibrosis. Semin Liver Dis 37: 119-127, 2017.
22. Gao JH, Wen SL, Tong H, Wang CH, Yang WJ, Tang SH, Yan ZP, Tai Y, Ye C, Liu R, *et al*: Inhibition of cyclooxygenase-2 alleviates liver cirrhosis via improvement of the dysfunctional gut-liver axis in rats. Am J Physiol Gastrointest Liver Physiol 310: G962-G972, 2016.
23. Yu J, Hui AY, Chu ES, Go MY, Cheung KF, Wu CW, Chan HL and Sung JJ: The anti-inflammatory effect of celecoxib does not prevent liver fibrosis in bile duct-ligated rats. Liver Int 29: 25-36, 2009.
24. Tahan G, Eren F, Tarçin O, Akin H, Tahan V, Şahın H, Özdoğan O, İmeryüz N, Çelıkel Ç, Avşar E and Tözün N: Effects of a long-acting somatostatin analogue, lanreotide, on bile duct ligation-induced liver fibrosis in rats. Turk J Gastroenterol 21: 287-292, 2010.
25. Hui AY, Leung WK, Chan HL, Chan FK, Go MY, Chan KK, Tang BD, Chu ES and Sung JJ: Effect of celecoxib on experimental liver fibrosis in rat. Liver Int 26: 125-136, 2006.
26. Harris TR, Kodani S, Rand AA, Yang J, Imai DM, Hwang SH and Hammock BD: Celecoxib does not protect against fibrosis and inflammation in a carbon tetrachloride-induced model of liver injury. Mol Pharmacol 94: 834-841, 2018.
27. Pinzani M: Epithelial-mesenchymal transition in chronic liver disease: Fibrogenesis or escape from death? J Hepatol 55: 459-465, 2011.
28. Lee SJ, Kim KH and Park KK: Mechanisms of fibrogenesis in liver cirrhosis: The molecular aspects of epithelial-mesenchymal transition. World J Hepatol 6: 207-216, 2014.
29. Tsubakihara Y and Moustakas A: Epithelial-mesenchymal transition and metastasis under the control of transforming growth factor β. Int J Mol Sci 19: 3672, 2018.
30. Baulida J, Díaz VM and Herreros AG: Snail1: A transcriptional factor controlled at multiple levels. J Clin Med 8: 757, 2019.
31. Scholten D, Osterreicher CH, Scholten A, Iwaisako K, Gu G, Brenner DA and Kisseleva T: Genetic labeling does not detect epithelial-to-mesenchymal transition of cholangiocytes in liver fibrosis in mice. Gastroenterology 139: 987-998, 2010.
32. Taura K, Iwaisako K, Hatano E and Uemoto S: Controversies over the epithelial-to-mesenchymal transition in liver fibrosis. J Clin Med 5: 9, 2016.
33. Pinheiro D, Dias I, Ribeiro Silva K, Stumbo AC, Thole A, Cortez E, de Carvalho L, Weiskirchen R and Carvalho S: Mechanisms underlying cell therapy in liver fibrosis: An overview. Cells 8: 1339, 2019.
34. Tsuchida T and Friedman SL: Mechanisms of hepatic stellate cell activation. Nat Rev Gastroenterol Hepatol 14: 397-411, 2017.
35. Fabregat I, Moreno-Càceres J, Sánchez A, Dooley S, Dewidar B, Giannelli G and Ten Dijke P; IT-LIVER Consortium: TGF-β signalling and liver disease. FEBS J 283: 2219-2232, 2016.
36. Chen YL, Lv J, Ye XL, Sun MY, Xu Q, Liu CH, Min LH, Li HP, Liu P and Ding X: Sorafenib inhibits transforming growth factor 1-mediated epithelial-mesenchymal transition and apoptosis in mouse hepatocytes. Hepatology 53: 1708-1718, 2011.
37. Song Y, Zhao Y, Wang F, Tao L, Xiao J and Yang C: Autophagy in hepatic fibrosis. BioMed research international 2014: 436242, 2014.
38. Boya P, Reggiori F and Codogno P: Emerging regulation and functions of autophagy. Nat Cell Biol 15: 713-720, 2013.
39. Allaire M, Rautou PE, Codogno P and Lotersztajn S: Autophagy in liver diseases: Time for translation? J Hepatol 70: 985-998, 2019.
40. Ke PY: Diverse functions of autophagy in liver physiology and liver diseases. Int J Mol Sci 20: 300, 2019.
41. Tong M, Zheng Q, Liu M, Chen L, Lin YH, Tang SG and Zhu YM: 5-methoxytryptophan alleviates liver fibrosis by modulating FOXO3a/miR-21/ATG5 signaling pathway mediated autophagy. Cell Cycle 20: 676-688, 2021.
42. Kuscuoglu D, Bewersdorf L, Wenzel K, Gross A, Kobazi Ensari G, Luo Y, Kilic K, Hittatiya K, Golob-Schwarzl N, Leube RE, *et al*: Dual proteotoxic stress accelerates liver injury via activation of p62-Nrf2. J Pathol 254: 80-91, 2021.
43. Tan S, Liu X, Chen L, Wu X, Tao L, Pan X, Tan S, Liu H, Jiang J and Wu B: Fas/FasL mediates NF-κBp65/PUMA-modulated hepatocytes apoptosis via autophagy to drive liver fibrosis. Cell Death Dis 12: 474, 2021.
44. Song M, Zhang H, Chen Z, Yang J, Li J, Shao S and Liu J: Shikonin reduces hepatic fibrosis by inducing apoptosis and inhibiting autophagy via the platelet-activating factor-mitogen-activated protein kinase axis. Exp Ther Med 21: 28, 2021.
45. Dikic I and Elazar Z: Mechanism and medical implications of mammalian autophagy. Nat Rev Mol Cell Biol 19: 349-364, 2018.
46. Fukui H, Saito H, Ueno Y, Uto H, Obara K, Sakaida I, Shibuya A, Seike M, Nagoshi S, Segawa M, *et al*: Evidence-based clinical practice guidelines for liver cirrhosis 2015. J Gastroenterol 51: 629-650, 2016.
47. Yoshiji H, Nagoshi S, Akahane T, Asaoka Y, Ueno Y, Ogawa K, Kawaguchi T, Kurosaki M, Sakaida I, Shimizu M, *et al*: Evidence-based clinical practice guidelines for Liver Cirrhosis 2020. J Gastroenterol 56: 593-619, 2021.